THE INTERACTION OF RADIATION WITH AEROSOL

by A Slingo

1. Introduction

The purpose of this lecture is to give an introduction to the ways in which electromagnetic radiation interacts with aerosol in the atmosphere. By aerosol we mean any small particles in solid or liquid phase, which therefore includes haze, dust, cloud and fog droplets, rain, hail, ice crystals and even air molecules themselves. The optical properties of such aerosols are a function of their composition and shape, and the range of optical phenomena they exhibit is also determined by their size relative to the wavelength of the incident radiation. This latter constraint is very important and results in a unity between otherwise unrelated fields; for example the scattering of visible light by air molecules and that of microwaves by precipitation are both accounted for by Rayleigh scattering theory.

The application of the general results presented here to both meteorological research and practical techniques will be stressed, but of necessity some important overlap areas have been ignored. There will be little discussion of radiative transfer and none of the absorption of radiation by gaseous constituents.

2. Definitions

Basic definitions

r Radius of particle
λ Wavelength of incident radiation
x Dimensionless size parameter, $x = kr$, where $k = 2\pi/\lambda$
θ Scattering angle between scattered and incident radiation.

Most aerosols are partial absorbers of electromagnetic radiation, so that a fraction of the incident field is absorbed, to be re-emitted or dissipated as heat, and the remainder is scattered. A parallel beam of radiation of initial intensity I_0 will be attenuated to I after passing a distance L through a medium of such aerosols, according to the equation;

$$I = I_0 \exp\left\{-\int_0^L \beta_{EXT}\, dl\right\} \qquad -(1)$$

where β_{EXT} is known as the volume extinction cross section, with units length^{-1}, and the integral $\int_0^L \beta_{EXT}\, dl$ is known as the optical depth τ. The optical depth is a dimensionless quantity and as such is very useful in the theory of radiative transfer, as the equations can be written very generally in non-dimensional form.

The volume extinction cross section may be used to determine the meteorological range V using Koschmieder's formula;

$$V = \frac{3.912}{\beta_{EXT}} \qquad -(2)$$

The extinction of the radiation is composed of scattering and absorption so that we may write;

$$\beta_{EXT} = \beta_{SCAT} + \beta_{ABS} \qquad -(3)$$

The intensity and state of polarization of a plane electromagnetic wave can be described completely by four quantities which together form the Stokes vector $\begin{pmatrix} I_1 \\ I_2 \\ U \\ V \end{pmatrix}$. It is therefore possible to write down a simple vector equation which relates how the Stokes vector of the incident wave $\bar{F}(\theta) = \begin{pmatrix} I_1 \\ I_2 \\ U \\ V \end{pmatrix}$ is transformed to that of the scattered wave $\bar{S}(\theta) = \begin{pmatrix} I_{s_1} \\ I_{s_2} \\ U_s \\ V_s \end{pmatrix}$ by scattering from the aerosol;

$$\therefore \quad \bar{S}(\theta) = \beta_{SCAT} \cdot \frac{\bar{P}(\theta)}{4\pi} \cdot \bar{F}(\theta) \qquad -(4)$$

where $\bar{P}(\theta)$ is the 4 x 4 transformation or scattering matrix, determined by the size and composition of the aerosol. When unpolarized radiation is scattered from a spherically symmetric aerosol, the total intensity of the scattered radiation as a function of scattering angle is given by the phase function $p(\theta)$, which is simply related to the elements of $\bar{P}(\theta)$ and for most purposes contains all the information one needs on the angular distribution of the scattered field.

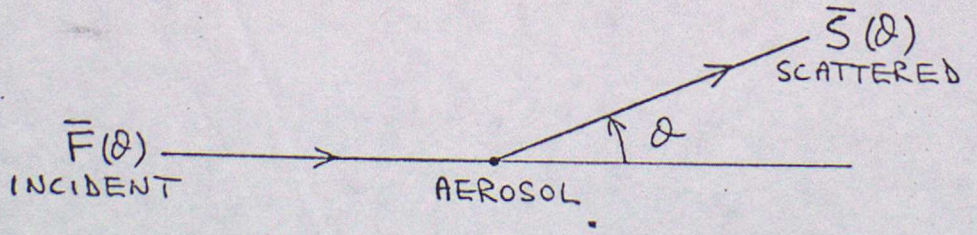

Fig. 1 Scattering geometry

There are three important regimes depending on the magnitude of the size parameter α. Firstly, when $\alpha \ll 1$ there is Rayleigh scattering, named after the papers by Lord Rayleigh which first appeared in 1871. The other extreme with $\alpha \gg\gg 1$ represents geometrical optics, in which the

particle is so much larger than the wavelength that ray-tracing techniques may be applied. Intermediate between these two is Mie theory, first published by G. Mie in 1908, which is the general theory of the scattering of radiation by spherical particles and which includes both extremes in its solutions. These will now be examined in turn.

3. Rayleigh scattering $(x \ll 1)$

The requirement that $x \ll 1$ ensures that a Rayleigh scatterer experiences a uniform applied electric field, to which is added the induced dipole field resulting from polarization of the particle. It is quite easy to show that for unpolarized incident radiation of intensity I_o, the scattered intensity I at distance a and angle θ from a spherical particle of radius r and refractive index m is given by;

$$I = (1 + \cos^2\theta)\left(\frac{m^2-1}{m^2+2}\right)\frac{16\pi^4 r^6}{\lambda^4}\frac{I_o}{a^2} \qquad \text{——⑤}$$

There are several important results summarised in this equation. Firstly, the intensity is proportional to λ^{-4}, so that the shorter wavelengths are scattered much more efficiently. Secondly, the intensity is proportional to the sixth power of the radius of the particle, which has important ramifications for the use of radar in the detection of precipitation. Finally, the phase function $p(\theta) = 3/4\,(1 + \cos^2\theta)$, which is slightly peaked in the forward and backward hemispheres. As shown on figure 2, the intensity is made up of two components, so that at $\theta = 90°$ the scattered radiation is fully polarized.

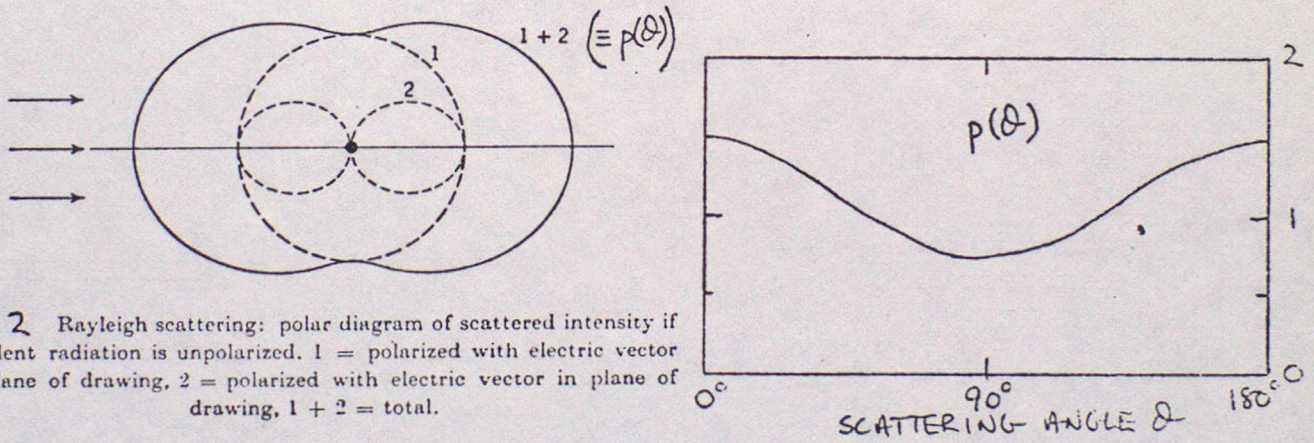

Fig. 2 Rayleigh scattering: polar diagram of scattered intensity if incident radiation is unpolarized. 1 = polarized with electric vector ⊥ plane of drawing, 2 = polarized with electric vector in plane of drawing, 1 + 2 = total.

The immediate application of these results was in the explanation of the blue colour of the sky. Atmospheric molecules are much smaller than the wavelength of visible light and act as Rayleigh scatterers. The light from the sun is unpolarized and, since the sun subtends an angle of only about $\frac{1}{2}°$, the incident radiation approximates to a plane wave. When looking away from the sun one sees light which has been Rayleigh scattered on average only once, and the λ^{-4} term ensures that this light is strongly biased towards the blue end of the spectrum. Careful measurements in clean atmospheres (free from the confusing contributions from the larger dust, haze and smoke particles) have shown that the intensity and polarization of skylight are close to the Rayleigh predictions, although there are deviations. For example, the light is not fully polarized at $\theta = 90°$ partly due to dust and the contribution from multiply scattered radiation which smears out this feature, and partly as a result of the finite size and anistropy of the molecules themselves. This requires an additional variable, the depolarisation factor δ, which for air has the value 0.0139 (Hoyt 1977). The volume scattering cross section

then becomes;

$$\beta_{EXT} = \frac{8\pi^3}{3\lambda^4}\frac{(m^2-1)^2}{N}\left(\frac{6+3\delta}{6-7\delta}\right) \qquad -(6)$$

where m is the refractive index of air and N the molecular number density. This equation enables the Rayleigh scattering properties of the atmosphere to be calculated from the known constants of air.

4. Geometrical optics - Rainbows and haloes $(x \gg\gg 1)$

a) Rainbows

Geometrical optics may be used in the explanation of the rainbow, which is caused by the refraction of sunlight through raindrops. A typical raindrop diameter is 1mm, for which the size parameter is about 10^4. This is so much larger than unity that ray-tracing techniques are applicable, in which the path of any given ray may be followed by applying the laws of refraction and reflection to the geometry of the aerosol. Several of the references give detailed discussions of the rainbow and its associated features. The scattering angles at which the primary and secondary bows are found are given by;

$$\theta = 2\phi - 2p\phi' \qquad -(7)$$

where $$\cos\phi = m\cos\phi' \qquad -(8)$$

and $\sin^2\phi = \frac{m^2-1}{p^2-1}$ for $p=2$ (Primary) and $p=3$ (Secondary) $-(9)$

the basic geometry for the primary rainbow is shown in figure 3.

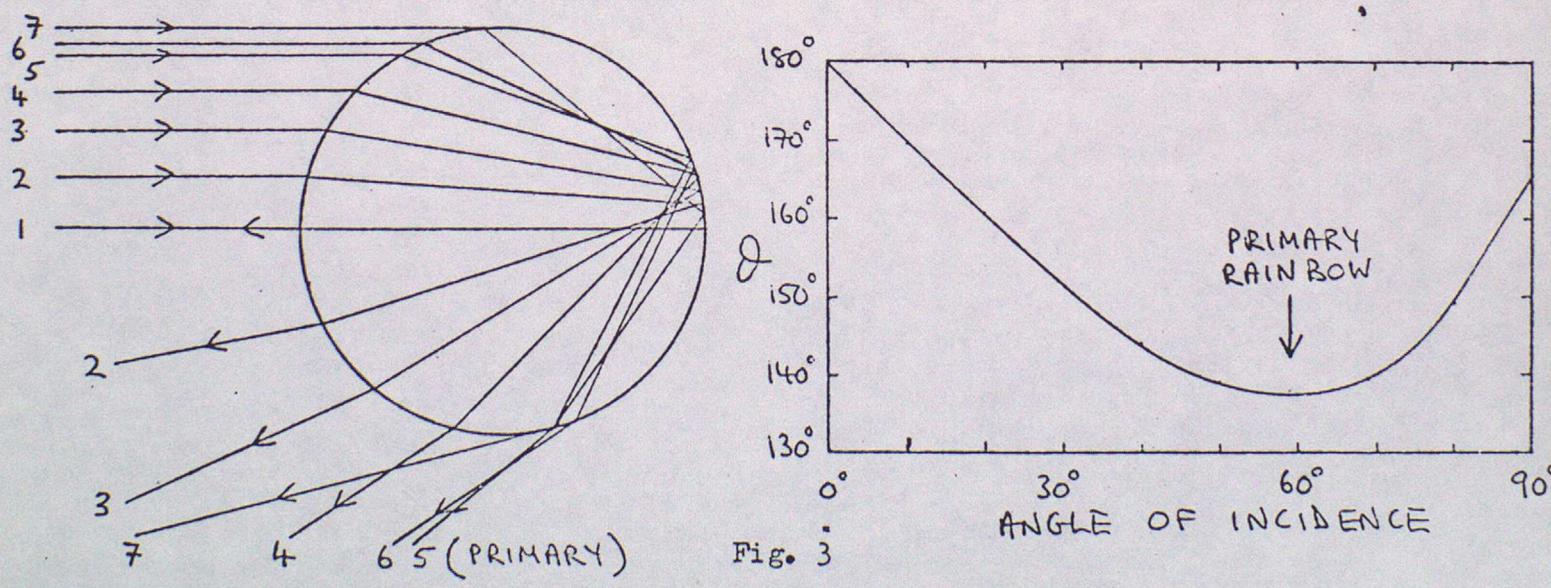

Fig. 3

It is important to remember that although geometrical optics may be used to derive the basic rainbow properties, detailed solutions require the full Mie theory. An example of the use of Mie theory is shown in figure 4, in which $p(\theta)$ is plotted for a narrow distribution of drizzle drops ($r = 100\mu m$). These solutions were obtained using a computer program which was written in support of the work in Met 015 on the radiative properties of clouds (Slingo and Schrecker 1980). The green and red curves are displaced downwards for clarity. The Primary is at the angle of minimum deviation for

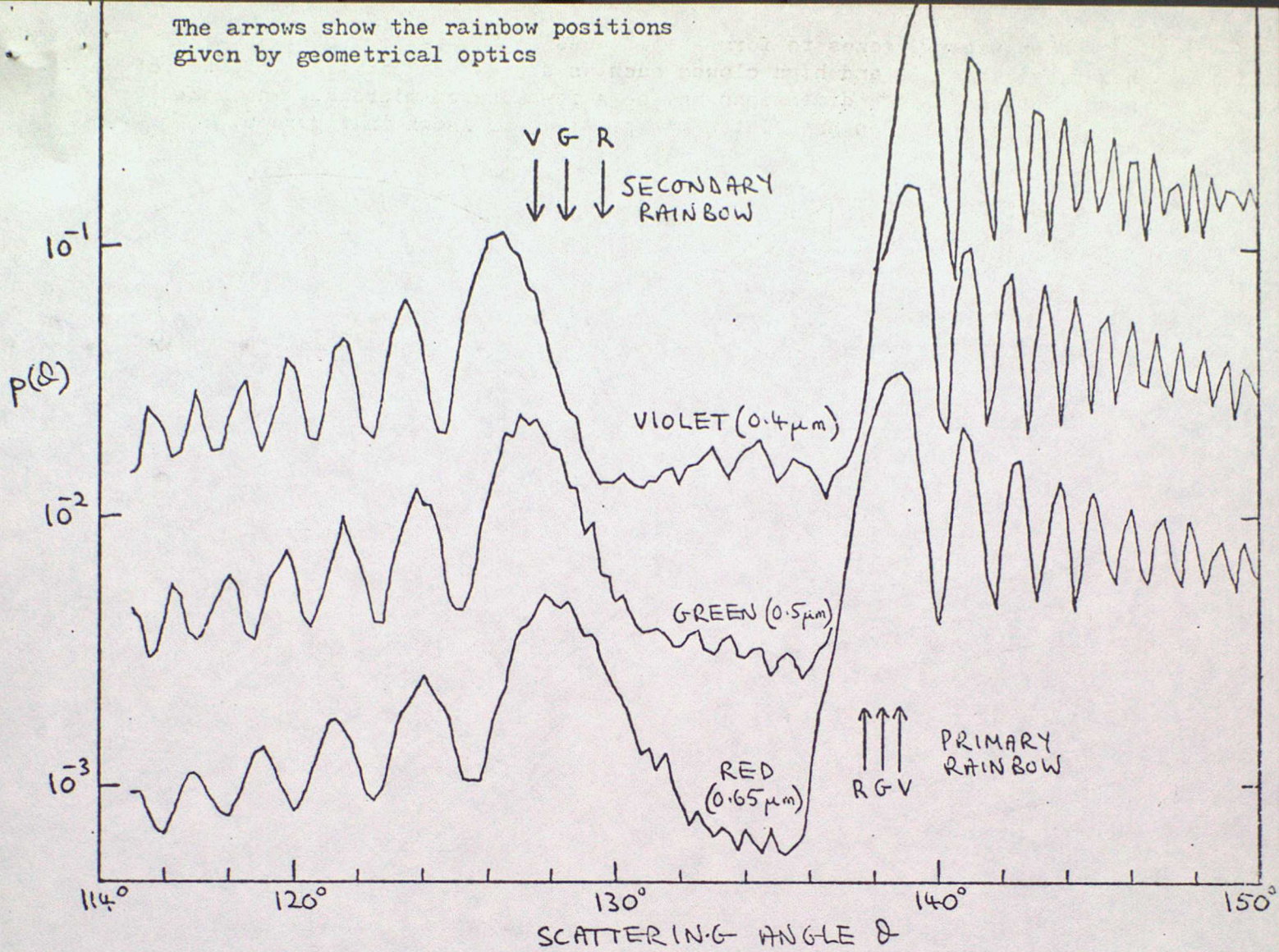

Fig. 4 Phase functions near the rainbow angles for three wavelengths

rays with one internal reflection and the resulting concentration of scattered light gives the intense bow. The refractive index of water is a function of frequency which displaces the maxima slightly, with Violet towards the anti-solar point ($\theta = 180°$) and Red on the outside of the bow. All rays away from the rainbow angle suffer a larger deviation, resulting in a bright background inside the bow and a dark background on the outside. Interference between two such rays with the same scattering angle (e.g. those marked 4 and 6 on figure 3) produces the "Supernumerary bows", which may often be seen just inside the Primary. These are especially striking in figure 4 due to the very narrow size distribution used. As the distance from the Primary increases, the supernumeraries merge together to form a white background. The Secondary rainbow is at the angle of maximum deviation for rays after two internal reflections. This bow is reversed in every way; the dark region is on the inside so that it reinforces that from the Primary, the colour sequence is reversed and the supernumerary bows are found on the outside, although these are so faint that they are rarely seen. The most noticeable effect of using 100 μm, as apposed to 1mm, drops in Figure 4 is a displacement and broadening of the rainbow maxima and supernumerary separations as compared to that normally seen.

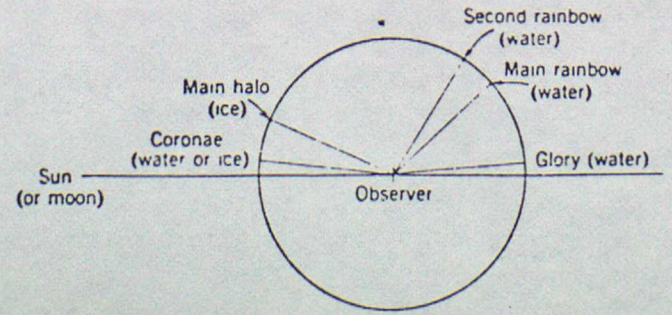

Fig. 5

The positions of the rainbows are shown schematically on figure 5, which also shows the ice halo which will now be described briefly.

When water freezes to form ice it does so in the form of regular hexagonal crystals and high clouds such as cirrus are entirely composed of such crystals, whose dimensions may be a few hundred microns. The most common crystal shapes are plates and pencils, as shown in figure 6.

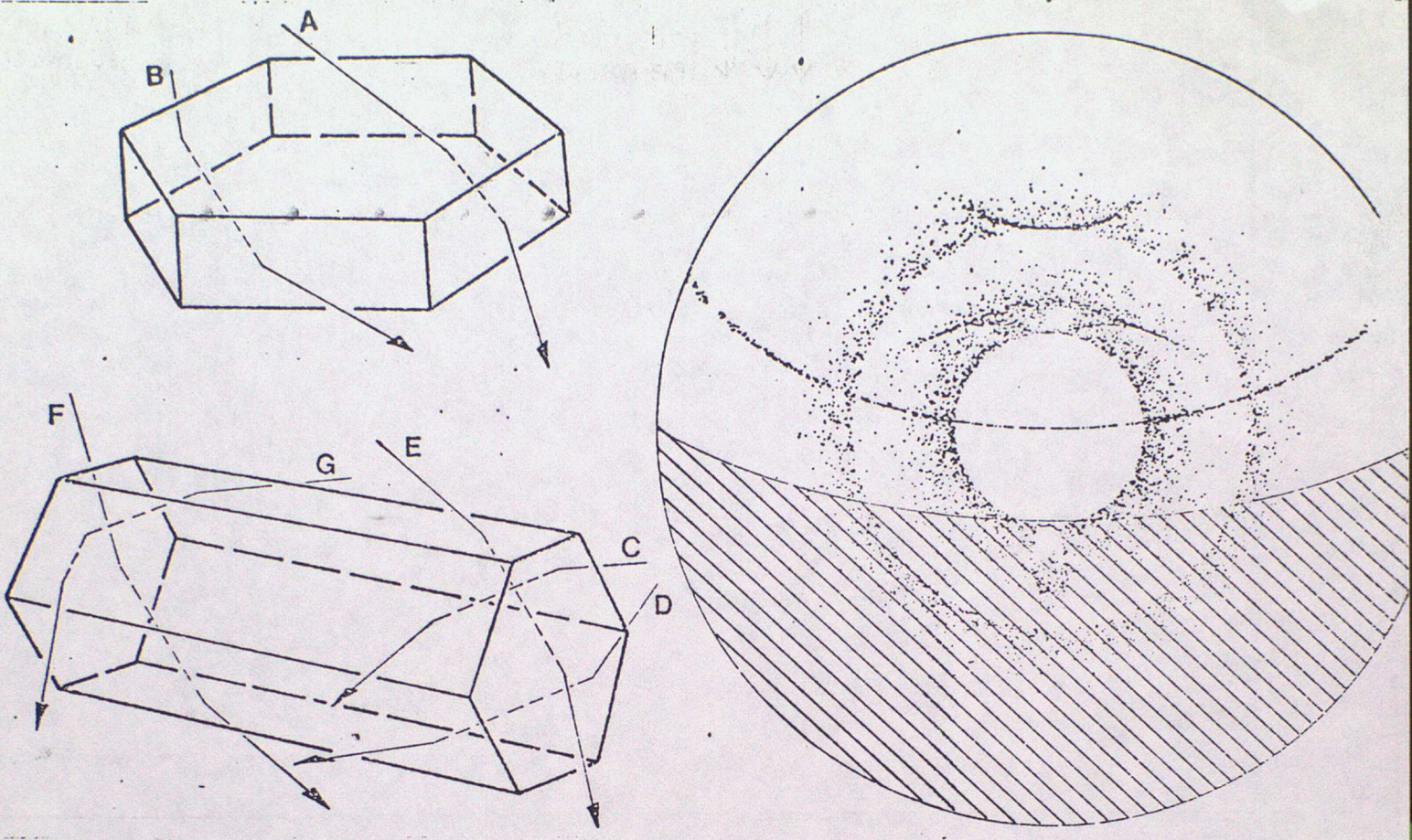

Fig. 6 Some of the rays responsible for ice crystal haloes

We have already seen that spherical raindrops produce complex rainbow features, and not surprisingly ice crystals can display an enormous range of halo phenomena. For details see the reference list. The most common haloes are the 22° halo, produced by rays B, C or D and the 46° halo, caused by A, E and F. The right hand diagram is a computer simulation of a halo display, with many other arcs also in evidence (Greenler et al. 1980).

5. Mie theory

Mie theory provides the general solution to the problem of the interaction of a plane electromagnetic wave with a spherical dielectric of arbitrary size. The solutions are obtained by a straightforward application of Maxwell's equations, with the appropriate spherical boundary conditions, and not surprisingly these constraints provide solutions containing Legendre polynomials and Bessel functions. These equations are complicated and will not be reproduced here. In the case of $x \gg 1$, a large number of terms are required in the expansions of these functions. It is only in the last decade or so that routine Mie theory calculations have become possible, because of the large CPU time required. The very complexity of the solutions can often be a hindrance, however, as it is not possible to identify each term with a recognisable physical effect. The formation of a rainbow, for example, may be expressed by thousands of terms and this is why simpler theories are often preferred, as they can provide much greater physical insight.

Figure 7 illustrates the polar diagrams of the scattered intensity as the size parameter x is increased from about unity. The polar diagram is initially nearly symmetric, as in Rayleigh scattering, but as x increases a strong forward peak appears, which becomes sharper and more intense, and

subsidiary maxima appear at other angles.

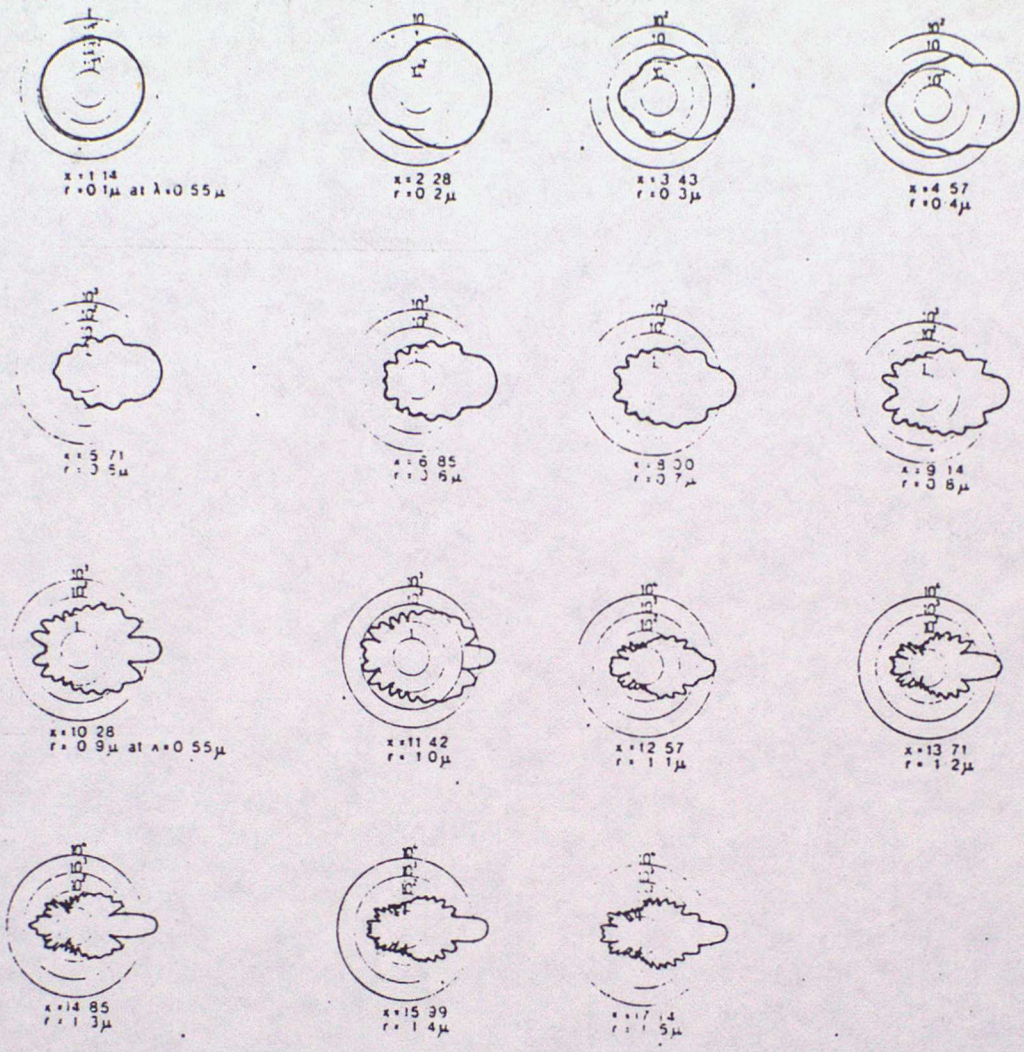

Fig. 7 Scattering polar diagrams. The size parameter $2\pi r/\lambda$ is indicated on the individual diagrams.

The forward peak is caused mainly by small angle diffraction around the edge of the aerosol, whereas the small backscatter peak and other features are due to rays which penetrate the sphere and those which creep around the outside as surface waves.

Some of the more important features in the phase function may be seen in figure 8, which has been calculated using data obtained recently by the MRF C-130 aircraft during a field study of maritime stratocumulus, as part of the JASIN experiment. The cloud droplet size distribution was measured with an ASSP, to be discussed later. The distribution was measured near cloud top, where the mode radius was about 10 μm and the liquid water content 0.7 gm^{-3} .

In calculating the Mie scattering properties of a distribution of drop sizes, the results are obtained by integrating the individual properties across the distribution. Great care has to be taken to use a small integration step, otherwise spurious peaks are created in the phase function. For visible light of wavelength 0.5 μm , used here, this requires considerable CPU time even on the IBM 360/195, as the mean size parameter is about 120. As mentioned above, the brilliant Aureole within a few degrees of the forward direction is caused by diffraction around the edges of the drops. The aureole is followed by a

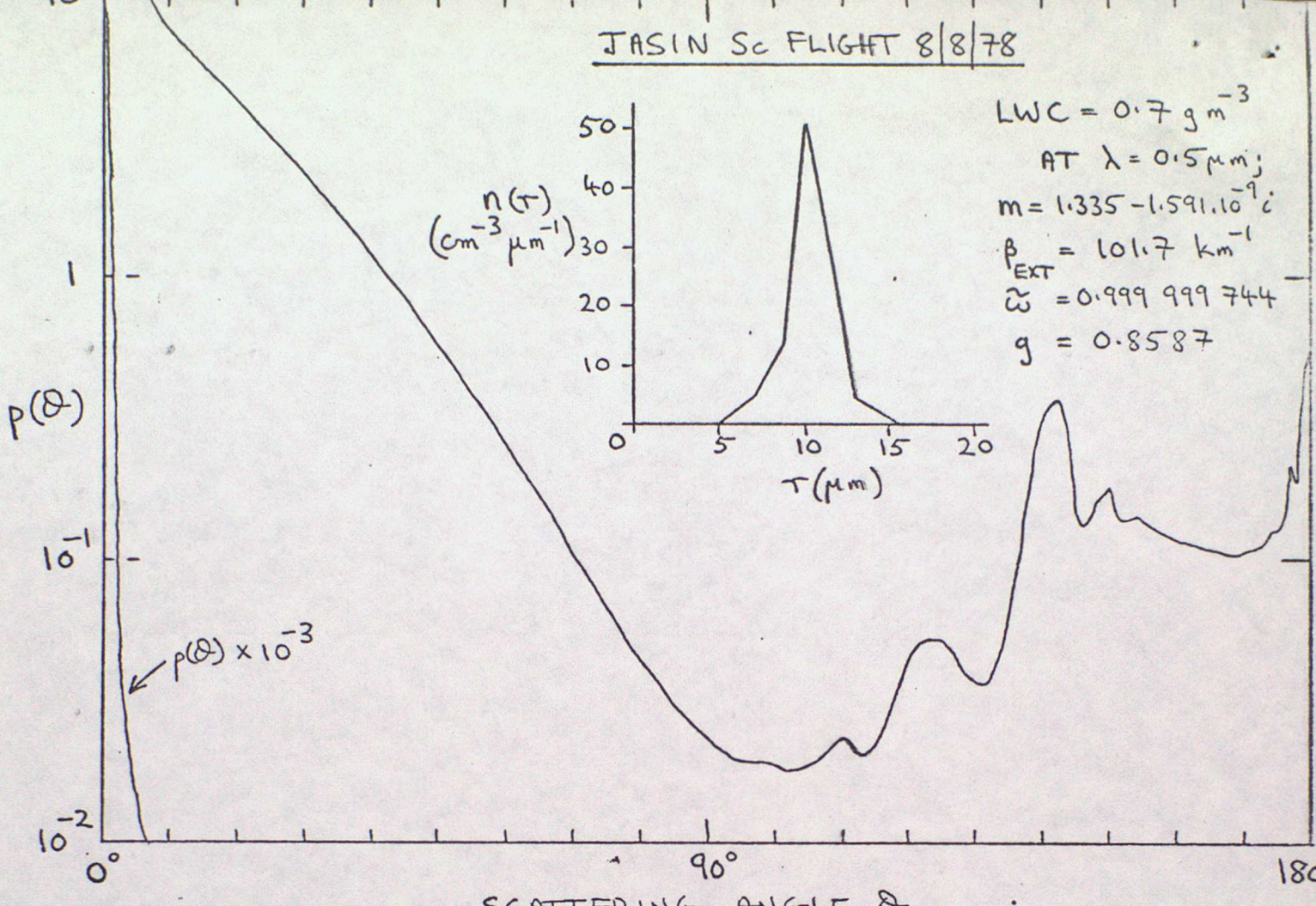

Fig. 8 Phase function for stratocumulus at $\lambda = 0.5\,\mu m$

slow decline through a region whose intensity is virtually independent of size distribution, an effect which is utilized by some types of particle counter. Intensity maxima are seen near the rainbow angles, but these are relatively smooth and broad. Such Cloudbows are rarely coloured and are usually seen as a white bow, or simply as a change in contrast. In the immediate vicinity of the backscatter direction are the highly detailed coloured rings of the Glory. This is often seen surrounding the shadow of an aircraft when projected onto cloud, and by mountaineers when the sun projects their shadow onto mist or cloud below them, when it is often known as the Brocken Spectre. An excellent example will be seen on the cover of the May 1979 issue of Weather. The complete explanation of the Glory is extremely complex. It is believed to be the result of interference between internally reflected rays of different polarizations, which have "skipped" part of the circumference of the drop as surface waves.

Note the large value of the extinction coefficient, so that for a cloud 1km thick the optical depth would be about 10^2. The visible optical depth can be estimated from the mode radius $r_m\ (\mu m)$ and liquid water content LWC $(g\,m^{-3})$;

$$\beta_{EXT} \approx \frac{1500 \cdot LWC}{r_m} \quad km^{-1} \qquad (10)$$

This works because for $x \gg 1$ the Mie theory functions approach their asymptotic (geometrical optics) limits. The extinction coefficient is nearly independent of wavelength, which is why clouds appear white. Also listed are the single scattering albedo $\tilde{\omega} = \beta_{SCAT} / \beta_{EXT}$, showing that only a very small fraction of the radiation is absorbed at this wavelength, and the asymmetry factor $g = 1/2 \int_0^{\pi} p(\Theta) \cos(\Theta) \sin(\Theta)\, d\Theta$, which gives the asymmetry of the scatter between forward and backward hemispheres.

6. Applications I - Radiative properties of Clouds

One important application of this background is in the study of the radiative properties of clouds, both from the point of view of calculating the radiative heating rates in cloudy atmospheres for numerical model investigations and in devising reliable methods for retrieving cloud and temperature data from satellite measurements. An immediate complication is that the visual optical depth is very high, often at least 10^2, which means that photons experience strong multiple scattering within the cloud. The cloud properties are therefore as much a function of the degree of multiple scattering as of the single scattering properties shown earlier. Multiple scattering smears out the phase function, so that if we imagine sinking down through a cloud layer, the direct beam is gradually attenuated as more and more radiation is scattered into the diffuse field, until only the almost isotropic diffuse field is left. This is common experience; on dull overcast days it is impossible to tell the direction of the sun. The very isotropy of the radiation field means that details of the phase function are unimportant in determining cloud properties, and many approximate methods have been devised using only β_{EXT}, $\tilde{\omega}$ and g as the basic variables (e.g. Paltridge and Platt 1976). More elaborate techniques, such as Monte Carlo methods, have been used in specific monochromatic applications, but these are far too time consuming for broad band applications, when another problem arises. In the near infrared $(\lambda = 1-5\,\mu m)$ water drops absorb appreciably in the same wavelength ranges as the strong water vapour absorption bands. Unravelling the interaction between the two has itself led to a large literature (see e.g. IAMAP 1977).

In the longwave spectral region $(\lambda = 5-200\,\mu m)$ the radiative properties are dominated by thermal radiation from the drops. The large optical depths mean that there is very little net transfer of radiation within the cloud, so that both upward and downward radiative fluxes are close to σT^4, where T is the local temperature. At the cloud top, however, there is an obvious asymmetry between the essentially black body radiation streaming up from the cloud and the downward clear-sky radiation, which is weaker partly because it comes from higher, cooler regions and also because there is very little downward radiation in the so-called "atmospheric window" $(\lambda \approx 8-12\,\mu m)$ (e.g. Roach and Slingo 1979). The drops at cloud top therefore cool efficiently to space in this band, resulting in a thin layer of strongly radiatively cooled air at cloud top. This has important effects on the heat budget and dynamics of the cloud, as described in a subsequent lecture. It also results in an additional term in the droplet growth equation, because the longwave cooling allows the drops to grow in size by condensation, even in an under-saturated environment (Roach 1976).

7. Applications II - Practical techniques

a) Weather Radar

Weather radar systems operate at centimetre wavelengths and are used mainly to detect rain and hail from fronts and severe storms. A typical value of the size parameter is therefore 0.1, so that for most purposes the scattering follows the Rayleigh laws. The strength of the radar return depends on the reflectivity factor Z. This is related to the backscatter intensity, whose functional dependence is the same as for β_{EXT}, so that from equation 5 we may write $Z \propto r^6$. Changing to diameter D and considering a distribution of raindrops $n(D)$;

$$Z = \int_0^\infty n(D)\, D^6\, dD \qquad \text{——(11)}$$

Marshall and Palmer found that, as the rainfall rate R increases, the rain-

drop distribution $n(D)$ tends to become flatter, according to the empirical law;

$$n(D) = 0.08\, e^{-\lambda D}, \text{ where } \lambda = 41 R^{-0.21} \quad \text{—— (12)}$$

Substituting 12 into 11 and evaluating the integral we find;

$$Z = 296\, R^{1.47} \quad \text{—— (13)}$$

In practice the most commonly used $Z-R$ relationship is $Z = 200\, R^{1.6}$. In theory one could use this to infer rainfall rate directly but the uncertainties and deviations from equation 12 are too great and a rain gauge network is usually needed to provide a calibration.

Radar displays are often contaminated by the "bright band" - an intense echo from the vicinity of the freezing level. This is caused by changes in the dielectric constant and fall speed as ice crystals begin to melt, and also the aggregations of snowflakes which then occur.

The use of a coherent transmitter (i.e. frequency stable and of narrow bandwidth) allows the Doppler shift of the returned pulse to be measured and hence one of the three velocity components can be determined. Some beautiful studies of the air motion within severe storms have been made by using two such systems as a so-called Dual-Doppler radar, and multiple Doppler radars are also feasible, although expensive.

b) Cloud Physics measurements

The theoretical phase function shown in figure 8 was calculated using data from an ASSP (Axially Scattering Spectrometer Probe). This uses the Mie scattering of laser light by the cloud drops to determine the drop size distribution, and it is amusing to note that these data and the same laws are then used in reverse to investigate the radiative properties of the cloud. The principle of the ASSP is shown in figure 9. Light from a He-Ne laser

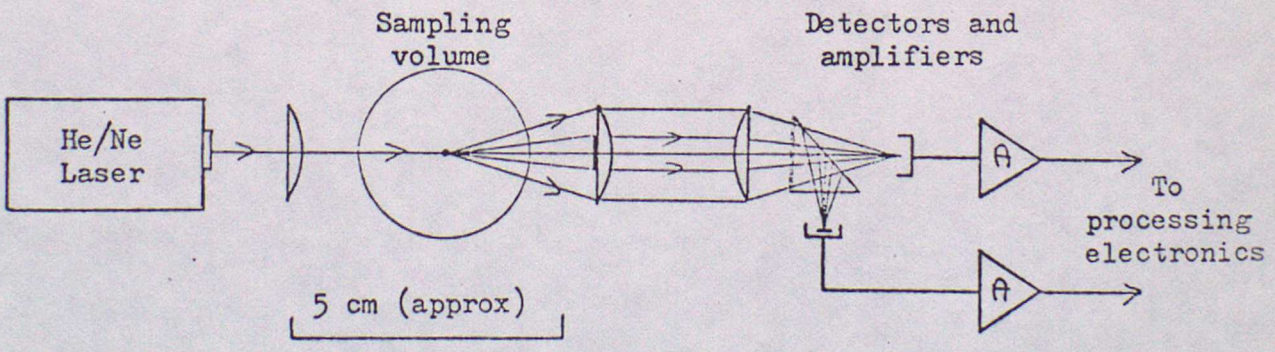

Fig. 9 Simplified block diagram of the ASSP

is focussed into the sampling volume, exposed to the airflow, where it is forward scattered into the sampling optics. The unscattered beam and light scattered with $\theta \leq 7^\circ$ are absorbed by the stop. An annular detector receives light with $7^\circ < \theta < 15^\circ$ and individual pulses as each drop traverses the beam are counted by the processing electronics. The intensity of the scattered light is proportional to the size of the drop, which allows the electronics to increment the count in one of 15 radius "bins", but it is also dependent on the location of the drop within the sensitive volume, so that some sophisticated logic is needed in the electronics to size the drops correctly, and this has required considerable work on the instruments operated by Met O 15.

References

General Textbooks

Deirmendjian D. 1969 Electromagnetic scattering on spherical polydispersions. Elsevier, New York.

van de Hulst H.C. 1957 Light scattering by small particles. John Wiley & Sons, New York.

McCartney E.J. 1976 Optics of the atmosphere. John Wiley, New York.

Tricker R.A.R. 1970 Introduction to Meteorological Optics. Elsevier/Mills and Boon, New York.

Twomey S. 1977 Atmospheric aerosols. Elsevier, Amsterdam.

Other references

Browning K.A. 1978 Meteorological applications of radar. Rep.Prog.Phys.41, 761-806.

Greenler R.G., Mallmann A.J. and Mueller J.R. 1980 Complex ice-crystal halo phenomena; Sky archaelogy. Weather,35, 346-353.

Hoyt D.V. 1977 A redetermination of the Rayleigh optical depth and its application to selected solar radiation problems. J.Appl.Met.16, 432-436.

IAMAP 1977 Standard procedures to compute atmospheric radiative transfer in a scattering atmosphere. IAMAP Radiation Commission Report, NCAR.

Paltridge G.W. and Platt C.M.R. 1976 Radiative processes in meteorology and climatology. Elsevier, Amsterdam.

Roach W.T. 1976 On the effect of radiative exchange on the growth by condensation of a cloud or fog droplet. Quart.J.R.Met.Soc.,102, 361-342.

Roach W.T. and Slingo A. 1979 A high resolution infrared radiative transfer scheme to study the interaction of radiation with cloud. Ibid.105, 603-614.

Slingo A. and Schrecker H.M. 1980 A computer program to calculate the properties of light scattered by a cloud of spherical particles. Met 015 Internal Report No. 11.